Clustering and magnetic anisotropy of Fe adatoms on graphene

C. D. Porter and D. Stroud

Phys. Rev. B **85**, 235452 — Published 25 June 2012

DOI: 10.1103/PhysRevB.85.235452

Clustering and Magnetic Anisotropy of Fe Adatoms on Graphene

C. D. Porter and D. Stroud

Department of Physics, The Ohio State University, Columbus, Ohio 43210, USA

Abstract

Single Fe adatoms and clusters of Fe adatoms on graphene are studied through first-principles calculations using density functional theory (DFT) and spin density functional theory (sDFT). First, we consider computational cells containing various numbers of C atoms and one Fe adatom. We calculate the binding energy, adatom height, and magnetic moment of the adatom above a few high-symmetry positions in the cell. In all cases, the binding energy increases with decreasing cell size, suggesting that clustering of the Fe adatoms is energetically favored. We also calculate the energy of various clusters of two to four Fe atoms on graphene in computational cells of various sizes, using both DFT and sDFT. These calculations again show that, both in DFT and sDFT, the Fe adatoms strongly prefer to form clusters. The energy barrier for an isolated Fe adatom to diffuse from the center of one graphene hexagon is calculated to be 0.49 eV. This barrier is reduced for an Fe atom which is one of a pair of neighboring adatoms. Finally, by including spin-orbit interactions within sDFT, we calculate the magnetic anisotropy energy of a single Fe adatom on graphene. We find that the in-plane anisotropy energy is close to zero, while the out-of-plane anisotropy energy is $\sim DS^2 \cos^2\theta$ where $S \sim 2.0$, θ is the angle between the magnetic moment and the perpendicular to the graphene plane, and $D \sim 0.25$ meV.

I. INTRODUCTION

In recent years, graphene (a two-dimensional honeycomb lattice of C atoms) has been extensively investigated[1–3] both for its many potential applications and for its unique physical properties. These potential applications run the gamut from photovoltaic cells[4] and ultracapacitors[5,6] to spin transport electronics[7]. Graphene also has many novel physical properties. These include a band gap of zero at the so-called Dirac point, a dispersion relation equivalent to that of massless Dirac fermions near the Dirac point, and low spin-orbit coupling. In addition to the intriguing characteristics of the continuous graphene sheet, the zig-zag edges of a graphene ribbon may allow only a single spin state for conduction electrons[8].

The presence of adatoms or impurities on graphene further influences its conductive and magnetic properties[9,10]. Such impurity atoms are almost always present as contaminants. They can also be introduced deliberately to tune the properties of the graphene sheet. For example, adsorbed F atoms produce a significant magnetic moment on the graphene C atoms[11], as can hydrogenation[12]. Adatoms also influence the electronic properties of graphene[13], e. g., by shifting the energy of the Dirac point, changing the density of states near that point, and altering electron and hole mobility[9].

The effects of isolated adatoms on graphene have also been investigated theoretically[14–16], largely using density functional theory (DFT) and related methods. Adatom binding energies on graphene, their heights above graphene, their effects on the local density of states (LDOS), and the effects of graphene on the magnetic moments of isolated adatoms have all been computed.

But little attention has been paid to clusters of two or more adatoms on graphene. There are several reasons for theoretically studying such clusters. First, several experiments[9,17] suggest that clusters do form in the case of Au and Ti adatoms. In some cases (e. g., Au[14]), such cluster formation may be aided kinetically by small energy barriers for adatom diffusion across the graphene. These indications of clustering are our main motivation for calculating the binding energies of small clusters of adatoms.

A second reason for looking at adatom clusters, especially of ferromagnetic species, is that any application of graphene to spintronics must include a ferromagnetic spin injector. The metal atoms in such a small electrical contact could diffuse across the surface if it were

energetically favorable, thereby influencing the electronic properties of the device. Furthermore, the adatom clustering could reduce the intended effects of the adatoms on the sheet conductivity. In either case, clustering could greatly affect the long-term device stability. Small ferromagnetic leads have been proposed[18] and established as spin injectors[19], and indeed, are already used in graphene-based spintronics devices[20–23].

In this work, we study Fe atoms and clusters adsorbed onto graphene using density functional theory (DFT)[24,25], and spin density functional theory (sDFT). Both are carried out using the generalized gradient approximation (GGA).

We also discuss the magnetic properties of Fe adatoms on graphene. Besides computing the magnetic moments of the adatoms as done previously[14], we approximately calculate the in-plane and out-of-plane magnetic anisotropy energies for an Fe adatom above the center of a graphene hexagon. We find that the in-plane anisotropy energy is approximately zero, while the out-of-plane anisotropy energy is small but positive, in the sense that the magnetic moment of an Fe adatom prefers to lie parallel to the graphene plane.

The remainder of this paper is organized as follows. In Section II, we give an overview of our computational methods. In Section III, we present our numerical results for single Fe atoms and clusters of Fe atoms on graphene. Section IV describes our method of estimating the magnetic anisotropy energy of a single Fe atom on graphene, and presents our calculated anisotropy parameters. Finally, in Section V, we give a concluding discussion.

II. OVERVIEW OF METHODS

In this work, we use primarily spin density functional theory (sDFT). In some instances we compare sDFT results to those obtained using the version of DFT in which the density of states is assumed to be the same for both spin up and spin down electrons (denoted simply DFT). For systems including Fe, sDFT is certainly more appropriate. DFT was employed to investigate whether a clustering preference might strongly depend on magnetic interactions.

In both cases, we use the Vienna Ab Initio Simulation Package (VASP)[26–29]. The ionic cores are modeled using either ultrasoft pseudopotentials (US-PPs)[30] or the projector-augmented wave method[31,32]. In some of our calculations, the positions of the ions were varied to minimize the overall free energy, while in others they were held fixed. If the ionic positions are varied, then between each ionic step the electronic states of the system are

relaxed self consistently to minimize the Kohn-Sham energy functional[24,25]. In this work, US-PPs were used for all calculations which did not include spin interactions, while the projector-augmented wave method of Perdew, Burke, and Ernzerhof (PAW-PBE)[33,34] was used for all sDFT calculations. Obviously, since Fe is a ferromagnetic element, calculations without spin interactions will be less accurate for Fe on graphene than those that include spin. They are presented here primarily to suggest that the clustering trends seen here are not unique to ferromagnetic elements. The two different models for ionic cores are used also to suggest the generality of this clustering tendency. Binding energies are significantly affected by the inclusion of spin, and by the choice of pseudopotential. Indeed, the binding energies obtained from the two types of calculations described (sDFT and DFT) differ quantitatively (by as much as 2.0 eV in the case of isolated adatoms). However, the fact that the binding energy per atom increases with clustering is consistent between the two methods.

All of our calculations are carried out using periodic boundary conditions, with wave functions expanded in plane waves. As a result, an adatom in the computational unit cell will interact with neighboring adatoms in the periodically repeating image cells, unless the computational unit cell is so large that this interaction can be neglected.

In our calculations, a constant 15-Å spacing has been used in the z-direction (perpendicular to the graphene sheet) to minimize cross-talk between the supercell and its image in the z-direction. The asymmetry of the supercell along the z axis can lead to a spurious dipole moment from image supercells. This spurious moment is reduced by the large supercell spacing in the z-direction, and is further eliminated within the framework of VASP.

At finite temperatures, partial occupancies of orbitals are specified by a Gaussian smearing scheme with the Gaussian width $\sigma = 0.05$. We included all plane waves in our calculations up to 500 eV The ionic relaxation was carried out using the conjugate gradient method. In most ionic relaxations the adatoms were taken to be above a high-symmetry position in the graphene unit cell, and in these cases all atoms in the supercell were allowed to move. In other cases, Fe adatoms were placed in off-symmetry positions in order to map the approximate binding energies during diffusion. In these cases some atoms were fixed in place, as discussed in Section III B. In all cases, the total energies per supercell were converged to within at least 0.01 eV and usually better. The convergence criterion was varied slightly, depending on supercell size and the type of calculation. For the anisotropy

calculations, the total supercell energies were converged to a precision of 10^{-8} eV .

III. CLUSTERING RESULTS

A. A Single Fe Atom Above a High Symmetry Point: Effect of Supercell Size

Before discussing adatom clustering, we first consider a single adatom above a graphene sheet. While many groups have investigated isolated adatom systems, little work has been done on systems with smaller supercells, such that nearest neighbor adatoms are separated by only 1-4 hexagon "diameters" (where the "diameter" means the distance between opposite edges of the hexagon). We will refer to pairs of nearest neighbor adatoms with such relatively small distances between nearest neighbors as "proximal adatoms". To investigate proximal adatoms, we use supercells consisting of 1, 2, 3, 4, 5, 6, and 16 graphene primitive cells.

The six smallest of these supercells are shown in Fig. 1. The smallest of these corresponds to one Fe adatom per graphene primitive cell, or a monolayer of Fe on graphene. The largest of these supercells corresponds to the case of fairly well isolated Fe atoms, which has already been studied by several groups[14,15].

Accurate ground state energies require adequate sampling of the Brillouin zone of the computational supercell with a grid of k-points. In order to ensure adequate k-space sampling, the k-point meshes used for these seven supercells had dimensions $30 \times 30 \times 1$, $24 \times 24 \times 1$, $21 \times 21 \times 1$, $18 \times 18 \times 1$, $18 \times 18 \times 1$, $15 \times 15 \times 1$, and $9 \times 9 \times 1$, respectively. Convergence tests showed that these sampling grids were adequate to ensure convergence. The $9 \times 9 \times 1$ grid has been used by other authors[14] on the supercell containing 32 C atoms.

Initially, these supercells were modeled using PAW-PBEs using sDFT. Later, for comparison purposes, the calculation was repeated using Ultrasoft Pseudopotentials (US-PPs) and DFT without spin[30,35], and at reduced k-space sampling. Here we present both sets of data, even though the PBE-systems with spin are clearly the more physically relevant of the two, especially for a transition metal adatom such as Fe. Both data sets are shown primarily because they demonstrate that the overall trends depend little on details of the computation such as pseudopotential choice. Comparison of the two data sets may also yield some insight into the role that magnetic effects play in the interaction energy between nearest neighbor Fe adatoms.

For each of the supercells shown in Fig. 1, the Fe adatom was placed in one of three high-symmetry positions within the unwarped graphene unit cell: above a hexagon center (denoted H position), above the center of a C-C bond (B), and directly above a C atom (T). The positions of all C atoms were allowed to relax. In some cases, the position of the Fe adatom was only allowed to relax in the z-direction (perpendicular to the graphene sheet), to prevent the adatom from changing relative positions (from B to H, for example). In each case, the binding energy E_B per adatom has been calculated according to

$$E_B = E_{bare} + E_{Fe} - E_{Fe+graphene}, \tag{1}$$

where $E_{Fe+graphene}$ is the energy per supercell of the relaxed system consisting of the Fe adatom and the graphene sheet, E_{bare} is the energy of one supercell of the bare, unwarped graphene sheet, and E_{Fe} is the energy of a single isolated Fe atom (in the absence of graphene). These binding energies are shown in Fig. 2 with spin (open symbols) and without spin (filled symbols). Binding energies are shown for supercells consisting of up to 12 C atoms. It was found that increasing supercell size beyond 12 C atoms yielded very little change in binding energy; this was numerically confirmed for supercells as large as 32 C atoms.

The nature of the bonding between the Fe and the graphene in the H position has been discussed previously in Ref.[14]. By calculating partial densities of states projected onto the Fe s, p, and d orbitals, and C s and p orbitals, they find that the bonding is primarily covalent and takes place between the Fe d orbitals and the C p states, as one might expect.

The preferred adatom height (that which minimizes the total energy) is displayed in Fig. 3 (only the more physically relevant case including spin is shown). The height is defined as the difference between the Fe ion z-position and the average z-position of all C atoms in the graphene sheet ($h = z_{Fe} - \langle z_{graphene} \rangle$). For the sDFT calculations done using the PAW-PBE pseudopotentials, the calculated magnetic moment μ per Fe adatom is shown in Fig. 4. μ is not the magnetic moment of the entire supercell; rather, it is the integral of the magnetization within a characteristic radius (1.30 Å for Fe) around the Fe adatom. The distinction is that this integral does not include any magnetic moments induced on the C atoms. For the supercell with 32 C atoms (not shown), $\mu \sim 2.03\mu_B$ for Fe in the H position.

B. A Pair of Fe Adatoms

The supercell calculations from Section (III A) do effectively include interactions among Fe adatoms in neighboring supercells. Furthermore, these interactions are attractive, because E_B increases with decreasing supercell size. This result can be interpreted as showing that the adsorbed Fe atoms prefer to cluster. In this section, we consider the tendency to cluster more explicitly, by calculating the binding energy of a single pair of Fe adatoms in the same supercell as a function of their separation. If the supercell is so large that the pair can be considered isolated from the image Fe adatoms in neighboring supercells, then the difference between the binding energy of the pair and that of two isolated adatoms represents the interaction energy between the two adatoms.

To calculate this difference, we considered two Fe adatoms, denoted α and β, which were placed in nearest neighbor hexagon centers within a graphene supercell. The total energy of this pair was calculated as adatom β was moved from the center of the nearest neighbor hexagon to the 3rd nearest neighbor hexagon center, as shown in Fig. 5. During these calculations, the C atoms were allowed to relax in all directions, while the Fe adatoms were allowed to relax in the z-direction only. Based on a full potential map of binding energies even in off-symmetry positions, we determined that the path of lowest potential barrier runs over the C-C bond center between the two hexagon centers. In order to isolate the single adatoms in one supercell from their periodic images in neighboring unit cells, it was found that a supercell containing 32 C atoms was sufficient in either DFT or sDFT. A picture of the 32-C atom supercell used is shown in Fig. 5. To calculate the binding energy as a function of separation, the two Fe adatoms were initially placed at the centers of adjacent hexagons, and then adatom β was moved as indicated by the black arrow in Fig. 5. The binding energy was calculated at each step. The results for the spin-independent and spin-dependent cases are displayed in Fig. 6. The cases in which the Fe adatoms are in nearest neighbor hexagons and third-nearest-neighbor hexagons are referred to as nnh and $3nnh$, respectively.

We briefly comment on these numerical results. First, in the DFT calculation, the binding energy of the pair is lower when β is above a bond center than a hexagon center. In the sDFT calculation, there is no obvious minimum in the binding energy when the second atom is at the B position, but E_B is still maximum when the two adatoms are in H positions in

adjacent hexagons. These results are also consistent with a preference of Fe adatoms to cluster.

If Fe adatoms prefer to cluster on graphene, one would expect that $E_{B,iso} < E_{B,pair} < E_{B,mono}$, where $E_{B,iso}$, $E_{B,pair}$, and $E_{B,mono}$ are the binding energies per adatom of an isolated adatom, a pair of adatoms in neighboring H positions, and a monolayer of Fe, respectively. Indeed we find that this relationship holds for both DFT and sDFT. The binding energies are listed in Table I for both nnh and $3nnh$ positions.

C. Three-Fe Cluster

Next, we consider a cluster of three Fe adatoms. The Fe adatoms were initially placed above the centers of adjacent graphene hexagons in a 32-C graphene supercell, so that they formed an equilateral triangle. All C atoms and Fe atoms were allowed to relax in all directions. For the (non-spin-dependent) DFT using US-PPs, the resulting binding energy per Fe atom was found to be 2.85 eV. All binding energies from this section are also listed in Table I. This binding energy per adatom is smaller than that found in a full monolayer, as expected. For the more realistic sDFT using PAW-PBEs, the binding energy per adatom is 1.89 eV, slightly larger than the value of 1.48 eV found earlier for pairs in sDFT, and in contrast to the ordering in the non-magnetic calculation. This result is consistent with other results suggesting that clustering is favored.

For comparison, we also calculated the binding energy of three Fe adatoms placed above C sites on adjacent graphene unit cells in the same 32-C supercell (T positions). The charge density of this arrangement is shown in Fig. 7(a). As in the previous calculation, all C atoms were allowed to relax in all directions. The binding energy per Fe atom was found to be 3.08 eV in DFT, greater than found for Fe adatoms above hexagon centers, but smaller than for Fe pairs as described in Section III B. In the case of sDFT, the binding energy per adatom with the Fe adatoms above C sites was found to be 2.07 eV. All the binding energies for the various three-atom clusters are also shown in Table I.

D. Four-Fe Cluster

A cluster of four Fe atoms is the smallest which can form an energetically stable three-dimensional cluster - a regular tetrahedron. This structure resembles the local structure of bulk Fe because the length of a bond between the centers of adjacent hexagons is within 1% of the distance between nearest neighbors in bcc Fe[36]. Below, we compare the binding energy of this cluster with that of a planar four-Fe cluster.

1. Fe Adatoms Above Hexagon Centers

We first considered four adatoms in-plane, using the same graphene supercell and methodology as in Section III C. The Fe atoms are arranged in a rhombus parallel to the graphene sheet, with the Fe atoms above the centers of adjacent graphene hexagons. All atoms were allowed to move in all directions. Using DFT, we find a binding energy per Fe adatom of 3.20 eV, which is larger than the binding energy in all other cases considered, except the monolayer. For sDFT, the binding energy per adatom is 2.16 eV.

We also considered a regular tetrahedral arrangement of Fe atoms, using the same supercell and settings as in Section III C. Again, the three Fe atoms at the base of the tetrahedron were positioned above the centers of adjacent hexagons. In this case, we found a binding energy of 3.77 eV using DFT. Once again, this is smaller than for Fe in a monolayer but larger than for either a pair of Fe adatoms or a cluster of three. Furthermore, the binding energy per adatom is larger for the tetrahedron than for the planar cluster of four Fe atoms, suggesting that Fe may prefer to form a three-dimensional rather than a two-dimensional cluster. The same trend was found using sDFT, for which the binding energy per adatom is 2.48 eV for a regular tetrahedron.

2. Fe Adatoms Above C Sites

Similar calculations were carried out for a cluster of four adatoms with the Fe atoms positioned in plane and above the C sites (T position). In this case the binding energy was found to be 3.41 eV using DFT, larger than for the four atoms above hexagon centers. In sDFT, the binding energy per adatom is 2.23 eV, which is also larger than for the four adatoms above hexagon centers. Analogous calculations were also carried out with the Fe

atoms arranged in a tetrahedron with the three base adatoms positioned above C sites. This arrangement yielded a binding energy of 3.61 eV using DFT and 2.44 eV using sDFT. These clusters are more strongly bound than the in-plane arrangement of four adatoms, again indicating a preference for clustering in three dimensions, and indicating that the H positions are preferred to the T positions for pyramidal clusters. All binding energies for the four-atom clusters are also shown in Table I.

IV. MAGNETIC PROPERTIES AND ANISOTROPY

In all our calculations so far, we have included no spin-orbit coupling (SOC). Even in the absence of SOC, many spin-dependent properties can still be discussed. These include the total magnetic moment on the adatom, the magnetic moments induced on the graphene atoms, and the tendency of adatoms to align ferromagnetically or antiferromagnetically.

The calculated total magnetic moment of each Fe adatom (within a characteristic radius of the ionic core as discussed before) is shown in Fig. 4 as a function of supercell size. These magnetic moments are generally lower for the H position than for the T or B positions. Furthermore, the moments in the T and B positions generally increase with supercell size, whereas the magnetic moment in the H positions generally decreases with supercell size to about 2.03 μ_B in the well-isolated case, as mentioned earlier

We also calculated the induced magnetic moments of the C atoms. These were computed, as with the Fe, by integrating the moment density from the nucleus out to a characteristic radius, in this case, of 0.863 Å. As one might expect, the moment induced on the C atom or atoms nearest to the Fe adatom are aligned antiparallel to that of the Fe adatom itself. This is true in all three high-symmetry cases. The moments on the C atoms farther from the Fe adatom seem to align parallel to the Fe magnetic moment, though they are smaller than those of the nearest neighbor carbons. This alternation of the induced magnetic moments is shown for the most energetically stable (H) position in Fig. 8. The figure is color-coded to show C atoms with antiparallel moments in red, and parallel in blue. The magnitudes of all the induced magnetic moments are very small compared to that on Fe itself: The largest magnitude of any induced moment on a single C atom, with Fe in the H position, is 0.019 μ_B. The total magnetic moment on the graphene, defined as the sum of the induced moments on all C atoms, is very small (always less than 0.1 μ_B per supercell). This would be consistent

with the so-called compensation theorem[37], which would give an induced moment of zero. Strictly speaking, however, this theorem only applies to a specific model of a localized spin interacting with a conduction electron gas, and not necessarily to the present calculation, which is based on spin density functional theory.

When a pair of adatoms are in the same supercell, the Fe moments are found to be ferromagnetically aligned. The largest collective magnetic moment observed for a pair was 6.15 μ_B in the nnh position and the lowest was 4.63 μ_B in the 3nnh position. The clusters of three and four also aligned ferromagnetically yielding net magnetic moments from 8.3 μ_B (three in T position) up to 10.4 μ_B (tetrahedral arrangement with base adatoms above H positions).

Although no arrangement of pairs of Fe adatoms was observed to align antiferromagnetically when fully relaxed, one can constrain spins in VASP and force them to lie antiparallel to one another. If one calculates the ground state energy of a pair of Fe adatoms in adjacent hexagons with their moments aligned and again antialigned (by such an artificial constraint), the difference between these two energies should yield an estimate of the magnetic interaction energy for this pair, within sDFT. We estimate this interaction energy to be 0.4 ± 0.1 eV. The uncertainty comes primarily from the choice of energetic penalty paid for small deviations of the spins from the antiferromagnetic arrangement. If the penalty is too small, the spins come out of their antiferromagnetic orientation; if the penalty is too large, even very small deviations from antialignment can lead to non-negligible contributions to the total calculated energy of the system.

In standard sDFT without spin-orbit interactions, as discussed thus far, the magnetic moments of all the electrons are all parallel or antiparallel to one axis. Because the overall Hamiltonian is invariant under a global rotation of spins, the total internal energy will be independent of the direction of this axis. The results presented in previous sections do indeed have this behavior.

If spin-orbit interactions are included, this rotational symmetry is broken and the energy of a system does depend on the direction of the magnetic moments. In VASP, such spin-orbit interactions can be included in the free energy functional to be minimized, and one can therefore estimate the magnetic anisotropy energies.

We have used this approach to calculate the magnetic anisotropy energy for an Fe adatom on graphene. Because C has a low atomic number, the spin-orbit coupling within graphene

is expected to be small. In VASP, the spin-orbit interaction is incorporated as an extra term in the Hamiltonian:

$$H_{SO} = \frac{\hbar^2}{2(m_e c)^2} \frac{1}{r} \frac{dV}{dr} \hat{L} \cdot \hat{S} \tag{2}$$

where V is the spherical part of the potential within the muffin tins surrounding each atomic nucleus, and $\hat{L}$ and $\hat{S}$ are the orbital and spin angular momentum operators (in units of $\hbar$). The matrix elements of the spin-orbit Hamiltonian have been estimated for graphene by a number of workers, often within a model tight-binding Hamiltonian[38–41] These matrix elements can be as large as 6 meV, but their effect on band splittings within the graphene band structure is typically found to be much smaller, perhaps of order 10^{-2}-10^{-3} meV.

To calculate the magnetic anisotropy of Fe on graphene, we constrained the Fe magnetic moment to lie along a specific axis and calculated the total energy (allowing the C spins to relax without constraints). This was done for many choices of the axis of the Fe magnetic moment, both within and out of the graphene plane. A 32-C supercell was used to isolate the adatoms from their neighboring images. The structure of the supercell was fully relaxed using sDFT before the spin-orbit coupling was added in. The orbital angular momentum, though we have not calculated it explicitly, also adjusts to its preferred value given the chosen direction of the spin magnetic moment.

To characterize the resulting anisotropy, we first note that, to second order in the spin operators, the excitations of a spin in an anisotropic environment can be described by the spin Hamiltonian[42,43]

$$H_{ani} = D\hat{S}_z^2 + G(\hat{S}_x^2 - \hat{S}_y^2) \tag{3}$$

where $\hat{S}_x$, $\hat{S}_y$, and $\hat{S}_z$ are quantum spin operators in units of $\hbar$ (they do not include any orbital angular momentum) . For particles with a large spin, the operators become approximately classical quantities. Thus in this limit, the Hamiltonian can be viewed as a potential energy for the spin in an anisotropic environment, which we can write as

$$E_{ani}(\theta, \phi) = DS_z^2 + G(S_x^2 - S_y^2) = S^2[D\cos^2\theta + G\sin^2\theta(\cos^2\phi - \sin^2\phi)] \tag{4}$$

Here θ and ϕ are the usual polar and azimuthal angles of the spin, measured respectively from a line normal to the graphene sheet and from a line drawn from the Fe atom to one of the nearest neighbor C atoms. Besides this term, there is a much larger portion of the Fe-graphene energy which does not depend on θ and ϕ. Assuming that form (4) applies to an

Fe atom on graphene, we can find the coefficients D and G by fitting the angle dependence of the total energy to this form, as we now describe. As will be seen below, the in-plane anisotropy is, in fact, zero to within our numerical accuracy; so the details of the in-plane analytic form are not important. The main numerical result is simply that the anisotropy energy varies as $DS^2 \cos^2\theta$.

To carry out this program, we calculated the total energy $E(\theta, \phi)$ from sDFT including spin-orbit interactions, for a range of θ and ϕ. Because the anisotropy energy is expected to be small, we calculated the total energy using a fine k-space mesh with dimensions $15 \times 15 \times 3$ and converged our calculations to within 10^{-8} eV, and then plotted various energy differences to obtain D and G.

Fig. 9 shows the calculated difference $E(90^o.\phi) - E(90^o, 0)$ as a function of ϕ for two supercell sizes containing 12 and 32 C atoms. In the larger cell, the energy is independent of ϕ to within at least 10^{-3} meV (filled symbols), while for the smaller cell, there is a weak ϕ dependence of order 0.05 meV. This dependence is undoubtedly due to spin-dependent interactions between the Fe atom and its images in neighboring supercells (which for the 12-atom supercell are rhombuses with vertex angles of 80^o and 100^o). Since the ϕ-dependence disappears for the larger cells, we conclude that the coefficient $G = 0$. The reason for using the 12-C supercell is to verify that the calculation is in fact sensitive to very small changes in energy due to anisotropy of the order 0.05 meV.

To determine D, we show in Fig, 10 the calculated energy difference $E(\theta, \phi) - E(0, 0)$ for an isolated Fe adatom on graphene (32 C atom supercell), plotted as a function of θ for two different values of ϕ. In both cases, the calculation shows that the energy is lowest when the moment lies in the xy plane ($\theta = 90^o$), indicating that $D > 0$. We obtain the coefficient D by using the fact that $G = 0$ and then writing $E(\theta, \phi) - E(0, 0) = D(\cos^2\theta - 1)S^2$. To obtain D we assume $S = 2$, since the calculated magnetic moment on the Fe adatom is very close to that integer value (2.03 μ_B). The value of D obtained in this way, for five different values of θ and two of ϕ, is $D = 0.255 \pm 0.001$ meV. Thus, the anisotropic part of the total energy, as calculated from sDFT including spin-orbit interactions, fits the form (4) to within 1% with $G = 0$. The positive sign indicates that the Fe magnetic moment prefers to remain in the plane of the graphene sheet. We were unable to find any previous measurement of the anisotropy energy of an Fe adatom on graphene for comparison with our calculations. However, Hirjibehedin *et al.* recently measured the out-of-plane anisotropy

term for Fe adatoms on the surface of CuN to be $D_{CuN} = -1.55$ meV. Given the small atomic number of C compared to Cu, our estimate that the anisotropy of an Fe atom on graphene is approximately one sixth that of CuN seems reasonable.

V. DISCUSSION AND CONCLUSIONS

A. Clustering of Fe Adatoms on Graphene

We have found strong evidence that Fe adatoms on graphene prefer to cluster. The evidence falls into two classes. First, the binding energy E_B per adatom increases with decreasing computational cell size. This shows that the Fe adatoms prefer to arrange themselves so as to have the highest possible number per unit surface area. This increase occurs for Fe adatoms in the preferred H site as well as in the metastable B and T positions, in both sDFT and DFT. Since Fe prefers to cluster in both sDFT and DFT, we conclude that the clustering preference does not much depend on magnetic interactions between adatoms.

Secondly, we have shown that for two or more Fe adatoms in a single computational cell, E_B generally increases with cluster size. As an example, for a pair of Fe adatoms in centers of adjacent hexagons, E_B is larger than that of an isolated Fe adatom by an amount of 0.73 eV per adatom in sDFT and by 1.07 eV in DFT.

In Table I, we show the calculated binding energies for Fe adatoms in a variety of configurations, as presented earlier in the paper. The notation has largely been discussed earlier. For the four-atom clusters, the description "in-plane" and "tetra" refers to planar and tetrahedral clusters. For energies of adatom pairs, *nnh* indicates that the two Fe adatoms are above nearest neighbor hexagon centers, and *3nnh* means they are above third nearest neighbor hexagon centers. In the case of pairs, *B* indicates that one of the two adatoms is above a C-C bond center while the other remains above a hexagon center.

Even if clustering of adatoms is favored energetically, it may be inhibited by diffusion barriers. For single Fe adatoms on graphene, this barrier is given by $E_{bar} = E_B(H) - E_B(B)$ in the limit of a large computational cell. This energy represents the lowest energy barrier for diffusion of an adatom from the center of one hexagon to the next. As can be seen from Fig. 2, this energy is about 0.9 eV in DFT and 0.3 eV for the more physically realistic sDFT for cells containing 12 C atoms. Our numerical results also give diffusion barriers for adatoms

which are members of a pair. For example, in Fig. 6 there is a diffusion barrier of about 0.2 eV, in DFT, and almost zero in sDFT, which must be overcome for an Fe adatom to move from the center of the third nearest neighbor hexagon (3nnh) to the nearest neighbor hexagon (nnh) position. Not only is this barrier very small in sDFT, but the binding energy per adatom is about 0.7 eV higher in the nnh position than in the 3nnh position.

All these results suggest that Fe adatoms have a strong energetic preference for clustering on graphene, and that the diffusion barrier inhibiting that clustering is reduced once the adatoms are in close proximity.

In our calculations of clustering, we have omitted possible corrections due to a finite Hubbard U, which might be expected to be relevant for a magnetic adatom such as Fe. Indeed, we recently became aware of work[44] showing that transition metal binding energies are significantly altered by the inclusion of a Hubbard U in the framework of VASP. For Fe, it is estimated that $U \sim 0.9$ eV[44–46]. We have carried out preliminary calculations including U and find that it does significantly change the binding energy of an Fe adatom (by as much as 0.44 eV). However, this change in binding energy seems not to affect the clustering tendency of Fe adatoms on graphene. More specifically, our initial calculations suggest that even with $U = 0.9$ eV, the lowest-energy position for an Fe adatom is still H.

Given the behavior of Fe, it would be interesting to consider the possible clustering of other species on graphene, both other transition metals, and non-magnetic adatoms. It has been experimentally observed, for example, that Au tends to cluster on graphene, and also that it diffuses readily along the surface[9]. The ease of diffusion implies that the diffusion barrier is small compared to that of Fe on graphene, perhaps because the p-d bonding of Fe on graphene mentioned earlier[14] does not occur for Au on graphene. Indeed. the work of Ref.[14] shows that the binding energy of a single Au impurity depends little on its position within the unit cell, implying a small activation energy for diffusion. To confirm a clustering tendency for Au adatoms, one would need to carry out total energy calculations such as those described here for Fe.

The strong preference of Fe adatoms to remain nearest neighbors indicates that Fe may be a good material for ferromagnetic leads on graphene. In this respect, it would be interesting to compare the binding energies, barrier energies, and energies of Fe clusters to those of alternative magnetic adatoms such as Co and Ni, which might also be used for spin injection. Furthermore, if the Fe adatoms do cluster as predicted here, this should significantly affect

electronic, and especially spin, transport in graphene, since scattering of electrons and spins from Fe impurities would be substantially affected by clustering.

We expect that the tendency of other species to cluster would be influenced by several factors, including the type of bonding between the adatom and graphene, and the degree of lattice constant matching between the graphene and a solid composed of the adatoms. A computational survey of adatoms with a good lattice match, and some with a poor match (K is an example), would be useful. One could then determine if the clustering tendency of the adatoms is primarily due to their bulk crystal structure and lattice constant.

B. Magnetic Anisotropy Energy

Our calculated magnetic anisotropy of Fe adatoms in the H position on graphene is consistent with eq. (4), with $G = 0$ to an excellent approximation. Moreover, the calculated out-of-plane anisotropy is very well modeled by this equation, with $D \sim 0.25$ meV.

Our calculations of magnetic anisotropy energy are oversimplified in at least two ways. First, we are including spin-orbit interactions through perturbation theory, as incorporated in VASP. Ideally, it would be better to include these effects by a fully relativistic calculation, as done, for example, in Ref.[42]. But since the substrate has a low atomic number for Fe on graphene, spin-orbit interactions are likely to be small, and the present simplified approach may be adequate. Secondly, corrections due to a finite U might be important, as mentioned above. We have not extended our magnetic anisotropy calculations to include a finite U, but such a calculation is feasible.

It would also be of interest to test these anisotropy predictions experimentally. This could possibly be done by measuring spin excitation energies experimentally, as was done in Ref.[42]. Likewise, it would be of interest to extend our anisotropy calculations to other transition metal adatoms on graphene.

VI. ACKNOWLEDGMENTS

This work was supported by by the Center for Emerging Materials at The Ohio State University, an NSF MRSEC (grant number DMR-0820414). We are grateful to Wolfgang Windl and Oscar Restrepo for valuable conversations about computations involving impuri-

ties on graphene, to Roland Kawakami for discussing his experimental studies of adatoms on graphene, and to Mario Badal, Michael Fellinger, and Jeremy Nicklas for useful discussions about computational methods..

[1] K. S. Novoselov, A. K. Geim, S. Morozov, D. Jiang, Y. Zhang, S. V. Dubonos, I. V. Grigorieva and A. A. Firsov, Science **306**, 5696, 666-669 (2004).

[2] K. S. Novoselov, A. K. Geim, S. V. Morozov, D. Jiang, M. I. Katsnelson, I. V. Grigorieva, S. V. Dubonos and A. A. Firsov, Nature **438**, 7065, 197-200 (2005).

[3] C. Meyer Jannik, A. K. Geim, M. I. Katsnelson, K. S. Novoselov, T. J. Booth and S. Roth, Nature **446**, 7131, 60-63 (2007).

[4] X. Wang, L. Zhi, and K. Müllen, Nano Lett. **8**, 323-327 (2008).

[5] W. H. Liu, T. Dang, Z. H. Xiao, X. Li, C. Zhu, and X. Wang, Carbon **49**, 3, 884-889 (2011).

[6] M. D. Stoller, S. Park, Y. Zhu, J. An and R. S. Ruoff, Nano Lett. **8**, 10, 3498-3502 (2008).

[7] O. V. Yazyev, M. I. Katsnelson, Phys. Rev. Lett. **100**, 4, 047209 (2008).

[8] Y. W. Son, M. L. Cohen, S. G. Louie, Nature **444**, 7117, 347-349 (2006).

[9] K. M. McCreary, K. Pi, A. G. Swartz, W. Han, W. Bao, C. N. Lau, F. Guinea, M. I. Katsnelson, and R. K. Kawakami, Phys. Rev. B **81**, 115453 (2010).

[10] C. P. Herrero and R. Ramirez, J. Phys. D **43**, 255402 (2010).

[11] X. Hong, S. H. Cheng, C. Herding, and J. Zhu, Phys. Rev. B **83**, 085410 (2011).

[12] L. Xie, X. Wang, J. Lu, *et al.*, Appl. Phys. Lett. **98**, 193113 (2011).

[13] K. Pi, K. M. McCreary, W. Bao, W. Han, Y. F. Chiang, Y. Li, S. W. Tsai, C. N. Lau, and R. K. Kawakami, Phys. Rev. B **80**, 075406 (2009).

[14] K. T. Chan, J. B. Neaton, and M. L. Cohen, Phys. Rev. B **77**, 235430 (2008).

[15] L. Hu, X. Hu, X. Wu, C. Du, Y. Dai, and J. Deng, Physica B **405**, 3337-3341 (2010).

[16] Y. He, J. Zhang, Y. Wang, and Z. Yu, Appl. Phys. Lett. **96**, 063108 (2010).

[17] K. M. McCreary, K. Pi, R. K. Kawakami, Appl. Phys. Lett. **98**, 192101 (2011).

[18] K. -H. Ding, Z. -G. Zhu, and J. Berakdar, Phys. Rev. B **79**, 045405 (2009).

[19] For a review of early spin injection mechanisms, see, e. g., I. Zutik, J. Fabian, S. Das Sarma, Rev. Mod. Phys. **76**, 323-410 (2004).

[20] E. Hill, A. K. Geim, K. Novoselov, F. Schedin, and P. Blake, IEEE Trans. Magn. **42**, 2694 (2006).

[21] N. Tombros, C. Jozsa, M. Popincius, H. T. Jonkman, and B. J. van Wees, Nature **448**, 571 (2007).

[22] W. Han, K. Pi, W. Bao, K. M. McCreary, Y. Li, W. H. Wang, C. N. Lau, and R. K. Kawakami, Appl. Phys. Lett. **94**, 222109 (2009).

[23] S. Cho, Y. F. Chen, M. S. Fuhrer, Appl. Phys. Lett. **91** 123105 (2007).

[24] P. Hohenberg and W. Kohn, Phys. Rev. B **136**, B864 (1964).

[25] W. Kohn and J. L. Sham, Phys. Rev. **140**, A1133 (1965).

[26] G. Kresse and J. Hafner, Phys. Rev. B **47**, 558 (1993).

[27] G. Kresse and J. Hafner, Phys. Rev. B **49**, 14251 (1994).

[28] G. Kresse and J. Furthmüller, Comput. Mat. Sci. **61**, 15 (1996).

[29] G. Kresse and J. Furthmüller, Phys. Rev. B **54**, 11169 (1996).

[30] G. Kresse and J. Hafner, J. Phys.: Condens. Mat. **6**, 8245 (1994).

[31] P. E. Blöchl, Phys. Rev. B **50**, 17953 (1994).

[32] G. Kresse, and D. Joubert, Phys. Rev. B **59**, 1758 (1999).

[33] J. P. Perdew, K. Burke, and M. Ernzerhof, Phys. Rev. Lett. **77**, 3865 (1996).

[34] J. P. Perdew, K. Burke, and M. Ernzerhof, Phys. Rev. Lett. **78**, 1396 (1997).

[35] D. Vanderbilt, Phys. Rev. B **41**, 7892 (1990).

[36] N. W. Ashcroft and N. D. Mermin, *Solid State Physics*, (Holt, Rinehart, and Winston, New York, 1976).

[37] P. W. Anderson, Phys. Rev. **124**, 41 (1961); P. W. Anderson and A. M. Clogston, Bull. Am. Phys. Soc. **6** 124 (1961).

[38] H. Min, J. E. Hill, N. A. Sinitsyn, B. R. Sahu, L. Kleinman, and A. H. MacDonald, Phys. Rev. **B 74**, 165310 (2006).

[39] Y. Yao, F. Ye, X.-L. Qi, S.-C. Zhang, and Z. Fang, Phys. Rev. **B 75**, 041401(r) (2007).

[40] D. Huertas-Hernando, F. Guinea, and A. Brataas, Phys. Rev. B **74**, 155426 (2006).

[41] C. L. Kane and E. J. Mele, Phys. Rev. Lett. **95**, 226801 (2005).

[42] C. F. Hirjibehedin, C. Lin, A. F. Otte, M. Ternes, C. P. Lutz, B. A. Jones, and A. J. Heinrich, Science **317**, 1199 (2007).

[43] D. Gatteschi, R. Sessoli, and J. Villain, *Molecular Nanomagnets*, (Oxford Univ. Press, Oxford, 2006).

[44] T. O. Wehling, A. I. Lichtenstein, and M. I. Katsnelson, arXiv:1107.3012v1.

[45] I. V. Solovyev, P. H. Dederichs, and V. I. Anisimov, Phys. Rev. B **50**, 16861 (1994).

[46] V. I. Anisimov, F, Aryasetiawan, and A. I. Lichtenstein, J. Phys.: Condens. Matter **9**, 767

(1997).

Geometry	Spin (Y/N)	Position	$E_B(eV)$
Monolayer	N	T	5.0
		B	5.0
		H	4.39
	Y	T	3.43
		B	3.32
		H	3.43
Isolated	N	T	1.15
		B	1.19
		H	2.05
	Y	T	0.17
		B	0.26
		H	0.75
Pair	N	3nnh	2.80
		B	2.47
		nnh	3.12
	Y	3nnh	0.76
		B	0.78
		nnh	1.48
Three	N	T	3.08
		H	2.85
	Y	T	2.07
		H	1.89
Four	N	T planar	3.41
		H planar	3.20
		T tetra.	3.61
		H tetra.	3.77
	Y	T planar	2.23
		H planar	2.16
		T tetra.	2.44
		H tetra.	2.48

Table I: Calculated binding energies per Fe, E_B for various arrangements of adatoms. The geometries and positions are discussed more thoroughly in the text. A Y in the "Spin" column indicates that spin interactions have been included and PAW-PBEs have been used. N indicates that spin interactions have not been included and US-PPs have been used.

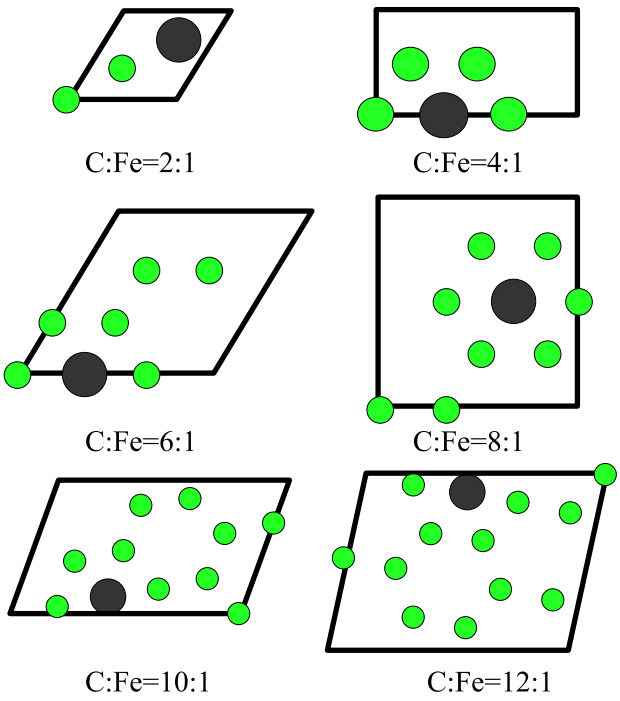

Figure 1: Computational supercells used in this work, each consisting of one Fe adatom and varying numbers of C atoms. C atoms are shown in green (small circles); Fe adatoms, in dark gray (large circles). The black lines indicate the boundaries of the computational unit cell.

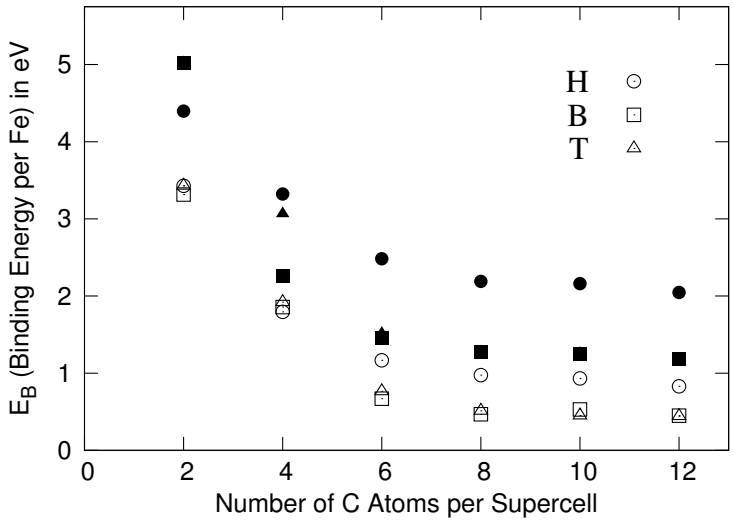

Figure 2: Calculated binding energies (in eV) for Fe adatoms on graphene for the three high-symmetry positions discussed in the text (H, B, and T, denoted respectively by circles, squares, and triangles), as functions of supercell size. The horizontal axis shows the number of C atoms in the supercell. Binding energies calculated from sDFT and DFT are marked by open symbols and filled symbols, respectively. Energies for the T and B positions are almost identical for some supercell sizes, and the corresponding filled symbols overlap in these cases.

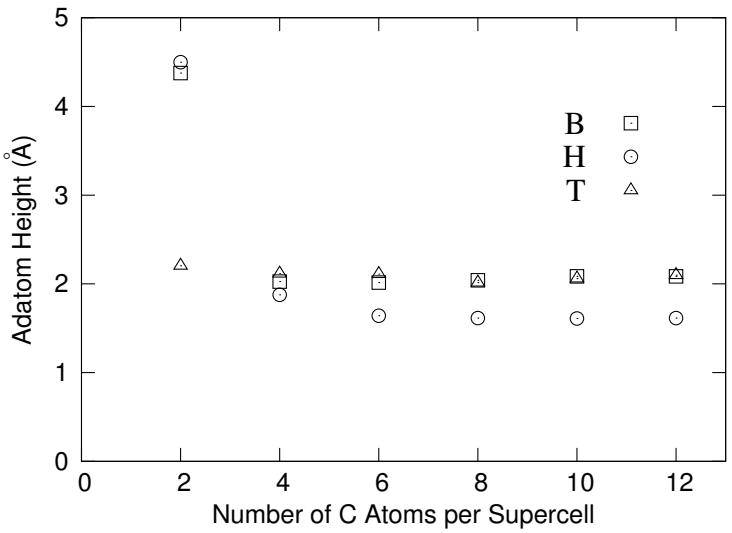

Figure 3: Calculated adatom heights (in Å) for Fe adatoms on graphene in the three high-symmetry positions described in the text (H, B, and T), as a function of computational supercell size using sDFT.

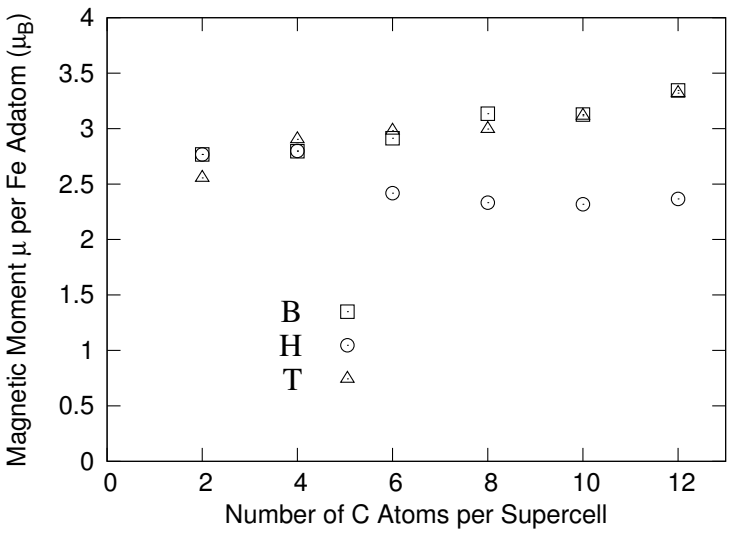

Figure 4: Calculated magnetic moments μ (in μ_B) for Fe adatoms on graphene in the H, B, and T positions, as a function of computational supercell size, as obtained using sDFT. Here μ is the integral over the moment density within a characteristic distance from the Fe nucleus (taken to be 1.30 Å for this calculation). $\mu \to 2.03\mu_B$ for H position and 32 C atoms/supercell (not shown in the figure).

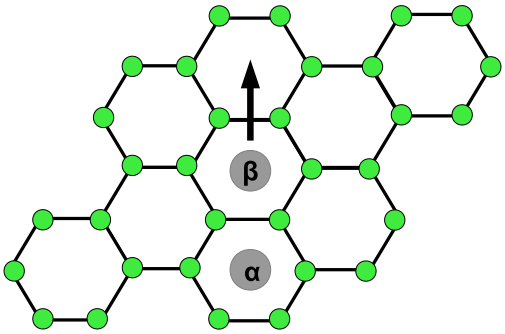

Figure 5: Schematic of a computational unit cell containing two Fe adatoms and 32 C atoms. Fe adatom α is kept fixed at the center of one hexagon. Adatom β is moved (vertically in the figure) away from adatom α in nine evenly spaced steps from the center of the nearest-neighbor hexagon to that of the third-nearest-neighbor hexagon, located at the tip of the vertical arrow. For a given α-β separation, all C atoms were allowed to move in all directions, and the two Fe atoms were allowed to move in the vertical direction, to obtain the binding energies shown in Fig. 6.

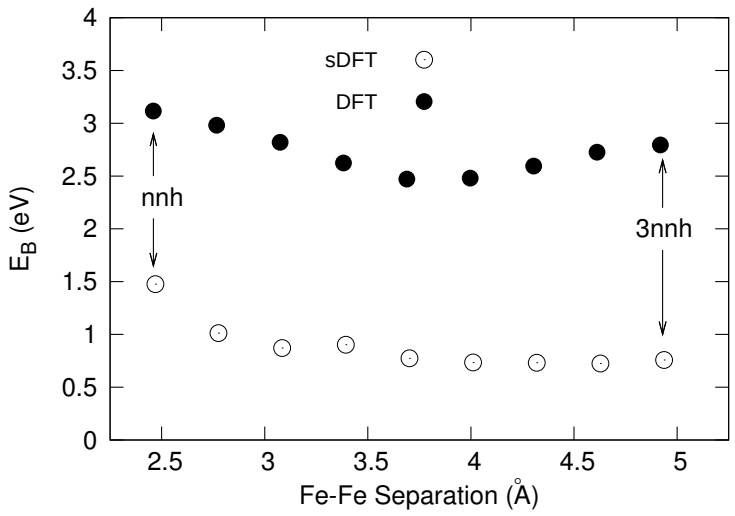

Figure 6: Calculated binding energy per adatom, E_B, for a pair of Fe adatoms on a 32-C graphene supercell. Energies are shown as calculated using sDFT (open symbols) and DFT (filled symbols). Their separation is varied as described in the caption to Fig. 5. At the position denoted "3nnh," atom β is located at the center of the third nearest neighbor hexagon.

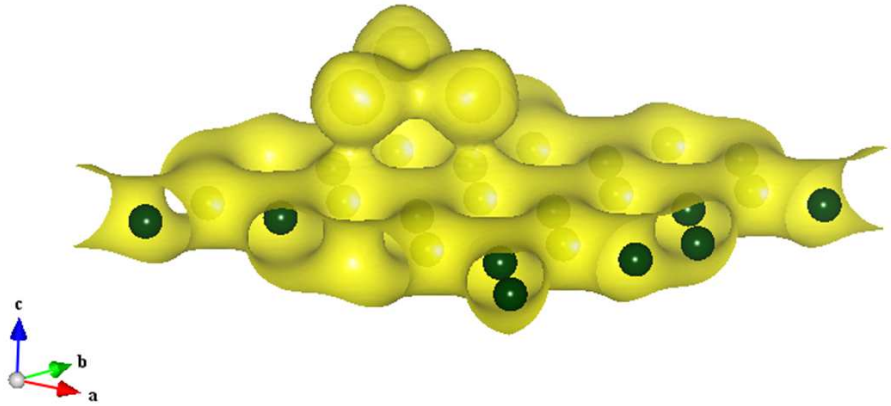

(a)Three adatoms

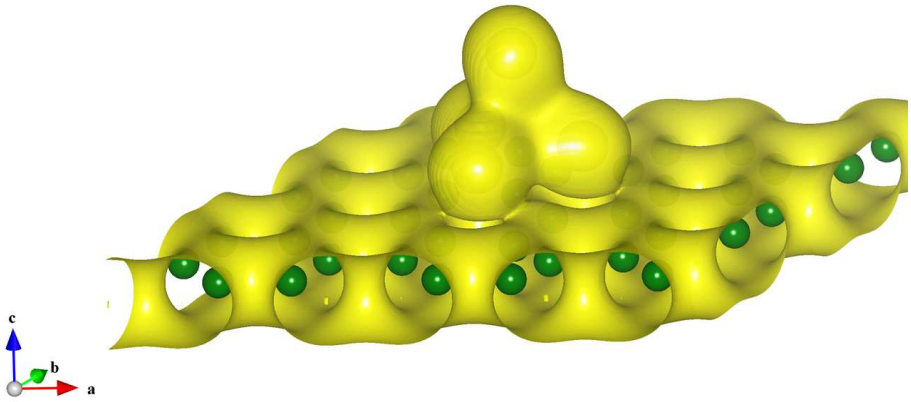

(b)Four adatoms (tetrahedral)

Figure 7: A calculated contour of constant electronic charge density for (a) a three-adatom arrangement and (b) a four-adatom tetrahedral arrangement of Fe on a sheet of graphene. The dark spheres inside the shell represent the centers of the C atoms; the Fe adatom cores are concealed behind the charge contour.

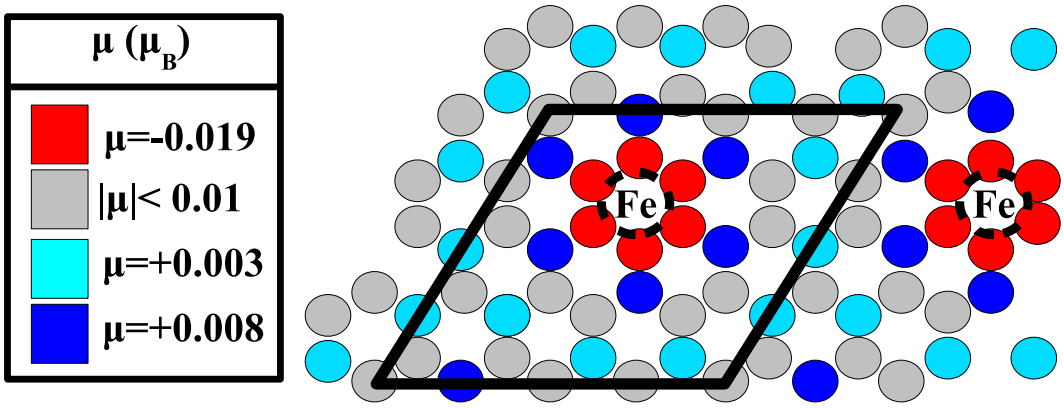

Figure 8: Magnetic moments induced on C atoms by an Fe adatom in the H position. The negative sign ascribed to the moments of the six nearest neighbor C atoms indicates that they are antiparallel to that of the Fe; a positive sign for other moments indicates parallel alignment. Rhombus indicates the computational unit cell.

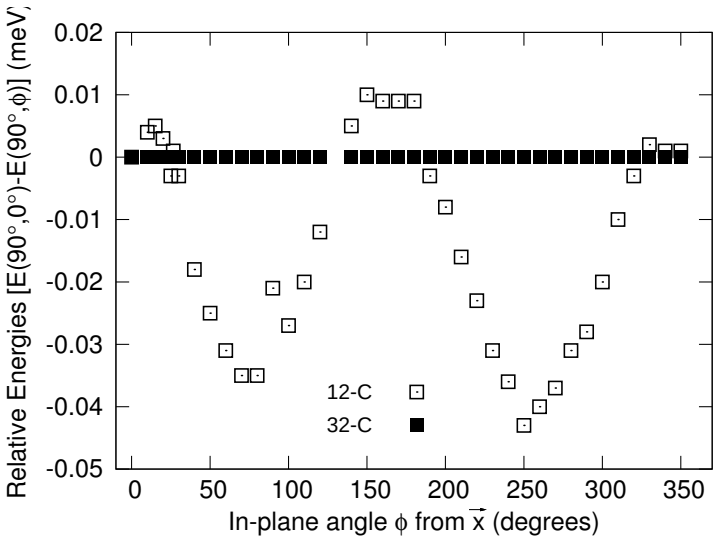

Figure 9: Energy difference $E(\theta = 90^o, \phi = 0) - E(\theta = 90^o, \phi)$ for an isolated Fe adatom on graphene (supercell containing 32 C atoms shown with filled symbols), and for a less isolated adatom (12 C atom supercell shown with open symbols), where $E(\theta, \phi)$ represents the total energy of a system in which the Fe moment has polar and azimuthal angles θ and ϕ. Both energy differences are plotted as functions of ϕ, holding θ fixed at 90^o (moment lying in xy plane). ϕ is the angle from the x axis, which is taken as a line from the Fe to a nearest neighbor C atom. The plotted energy difference is nonzero in the smaller supercell because there are residual magnetic interactions between the Fe adatoms and their neighboring images, as described in the main text.

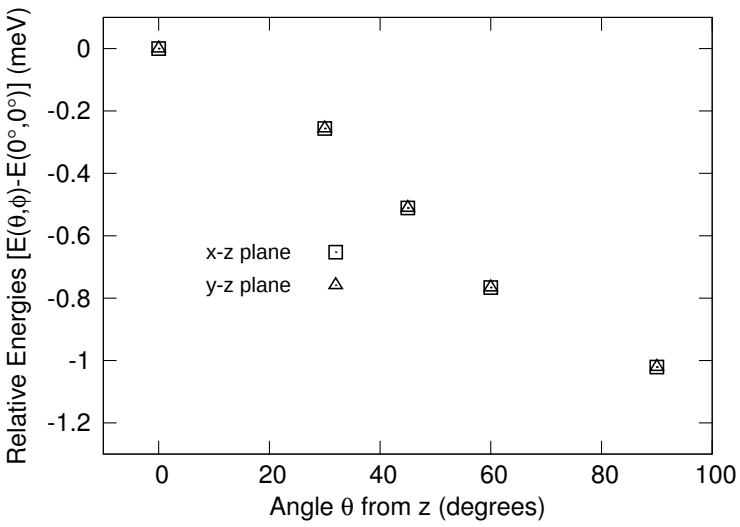

Figure 10: Calculated energy difference $E(\theta, \phi) - E(0, 0)$ for an isolated Fe adatom on graphene (32 C atom supercell), plotted as a function of θ for $\phi = 0$ (open squares) and $\phi = 90^o$ (open triangles). θ and ϕ represent the polar and azimuthal angle describing the orientation of the Fe magnetic moment. The orientation described by $\theta = 90^o$ and $\phi = 0$ corresponds to a moment pointing along the bond between the Fe and the nearest neighbor C atom. $phi = 0$ corresponds to a magnetic moment in the xz plane and $\phi = 90^o$ represents a magnetic moment in the yz plane, as indicated in the Figure. In both cases, the calculation shows that the energy of the moment is lowest when it lies in the xy plane ($\theta = 90^o$).